Research Article

Fangfang Wang, Ruoyu Hong*, Xuesong Lu, Huiyong Liu, Yuan Zhu, Ying Zheng, and David Hui

Improvement of long-term cycling performance of high-nickel cathode materials by ZnO coating

https://doi.org/10.1515/ntrev-2021-0020
received March 17, 2021; accepted April 1, 2021

Abstract: The high-nickel cathode material of $LiNi_{0.8}Co_{0.15}Al_{0.05}O_2$ (LNCA) has a prospective application for lithium-ion batteries due to the high capacity and low cost. However, the side reaction between the electrolyte and the electrode seriously affects the cycling stability of lithium-ion batteries. In this work, Ni^{2+} preoxidation and the optimization of calcination temperature were carried out to reduce the cation mixing of LNCA, and solid-phase Al-doping improved the uniformity of element distribution and the orderliness of the layered structure. In addition, the surface of LNCA was homogeneously modified with ZnO coating by a facile wet-chemical route. Compared to the pristine LNCA, the optimized ZnO-coated LNCA showed excellent electrochemical performance with the first discharge-specific capacity of 187.5 mA h g^{-1}, and the capacity retention of 91.3% at 0.2C after 100 cycles. The experiment demonstrated that the improved electrochemical performance of ZnO-coated LNCA is assigned to the surface coating of ZnO which protects LNCA from being corroded by the electrolyte during cycling.

Keywords: $LiNi_{0.8}Co_{0.15}Al_{0.05}O_2$, cathode material, ZnO coating, lithium-ion battery

1 Introduction

Since the first successful development and commercialization of lithium-ion batteries (LIBs) by Sony in Japan in 1991, LIB have received increasing attention [1]. Due to the high energy density, good cycling performance, and environmental friendliness [2], LIBs have become one of the most promising green secondary batteries in the twenty-first century [3]. As an important component of LIBs, the cathode material has much lower capacity than the anode material, accounting for the highest proportion of battery cost [4]. However, the initial Coulombic efficiency, rate capability, and cycling performance of these $LiNiO_2$-based cathode materials are not satisfactory, especially at an elevated temperature [5]. Therefore, research on high-capacity cathode materials plays a crucial role in the development of LIBs [6].

Among the layered materials, $LiNi_{0.8}Co_{0.15}Al_{0.05}O_2$ is a promising cathode material, which is due to the combination of the advantages of high theoretical capacity and stable layered structure of $LiNiO_2$ [7], $LiCoO_2$ [8], and $LiAlO_2$ [9]. As the precursor of $LiNi_{0.8}Co_{0.15}Al_{0.05}O_2$, $Ni_{0.8}Co_{0.15}Al_{0.05}(OH)_{2.05}$ is generally prepared by coprecipitation method [10]. However, the K_{sp} of $Al(OH)_3$ (4.57×10^{-33}) is much less than that of $Ni(OH)_2$ (2×10^{-15}) and $Co(OH)_2$ (1.58×10^{-15}), meaning that the ions of Al^{3+} precipitate faster with the hydroxide, which inhibits the uniform growth of the precursor [11]. The generated precipitate will undergo a lattice change and structural collapse during the cycling [12]. In the traditional preparation process, the oxidation of Ni^{2+} was carried out during the calcination [13]. However, the agglomeration of materials could make it difficult for the internal Ni^{2+} to be oxidized to N^{3+}, resulting in cation mixing [14]. The radius of Ni^{2+} is very close to Li^+, and the 3b of Ni^{2+} will occupy the 3a of Li^+ [15], which hinders the deintercalation of Li^+ and further affects the cycling performance. In addition, the Ni-containing cathodes easily react with electrolyte and the transition metal ions dissolve due to HF corrosion [16]. The unstable Ni^{4+} ions in the charged state tend to transform to more stable NiO on the cathode surface,

* **Corresponding author: Ruoyu Hong,** College of Chemical Engineering, Fuzhou University, Fujian 350000, Fuzhou, China, e-mail: rhong@fzu.edu.cn
Fangfang Wang, Huiyong Liu: College of Chemical Engineering, Fuzhou University, Fujian 350000, Fuzhou, China
Xuesong Lu: School of Engineering and Physical Sciences, Heriot-Watt University, Edinburgh EH14 4AS, United Kingdom
Yuan Zhu: EVE Energy Co., Ltd., Huizhou 516100, China
Ying Zheng: Department of Chemical and Biochemical Engineering, Western University, London, ON, N6A 5B9, Canada
David Hui: Department of Mechanical Engineering, University of New Orleans, New Orleans, LA 70148, United States of America

which results in high interfacial resistance and rapid capacity decay [17]. Moreover, the oxygen is released during the structural transition, causing poor safety performance of the battery [18]. Therefore, it is urgent for us to find a new strategy to solve these problems.

Doping aluminum has been found very effective to improve durability of LIBs because it stabilizes the charge-transfer impedance on the cathode. Much more effects have been paid to solve the problem of rapid precipitation of Al^{3+}. Trease *et al.* [19] used a series of techniques to measure the aluminum distribution in layered $LiNi_{0.8}Co_{0.15}Al_{0.05}O_2$ (NCA) to investigate the influence of aluminum doping on layer stabilization. The experimental results showed that Ni^{3+} ions incurred a dynamic Jahn–Teller (JT) distortion, while the Al reduced the strain associated with JT distortion by prioritizing the electron ordering of the JT long bonds of Al^{3+} ions. A new aluminum source, $NaAlO_2$, was employed by Liang *et al.* [20] to prepare a high-performance LNCA (LNCA-$NaAlO_2$). $NaAlO_2$ was hydrolyzed during the preparation of the precursor to avoid the rapid precipitation of Al^{3+} and the formation of flocculation precipitation. The obtained LNCA-$NaAlO_2$ with uniform element distribution and orderly layered structure showed a high initial discharge capacity of 204.7 mA h g^{-1} at 0.1C and a good capacity retention of 74.1% after 200 cycles. Zhou *et al.* [21] also used AlO_2^- as Al source to synthesize the Ni-rich precursor, $Ni_{0.9}Co_{0.07}Al_{0.03}(OH)_2$. After optimizing the calcination conditions, $LiNi_{0.9}Co_{0.07}Al_{0.03}O_2$ demonstrated excellent electrochemical performances. Kim and Kim [22] used acetylacetone as a chelating agent to effectively control the Al reaction rate, improve the uniform distribution of Al, and more importantly, increase the average particle size and density of NCA. Both the volumetric energy and specific capacity of LIBs were increased.

Many methods have been reported to improve such instable structural of high-nickel cathode material *via* doping and surface coating [23,24]. Liang *et al.* [25] found that the SiO_2 coating onto the surface of $LiNi_{0.8}Co_{0.1}Mn_{0.1}O_2$ can stabilize the layered structure, effectively reduce the corrosion of the cathode material by the electrolyte, and hence, improve the cycling performance. Liu *et al.* [26] used the pillaring effect of inactive Mg in the crystal structure to modify $LiNi_{0.8}Co_{0.1}Mn_{0.1}O_2$ by doping Mg and obtained the improved cycling stability (high-capacity retention of 81% over 350 cycles at 0.5C).

In this work, we report the synthesis, structural characterization, and electrochemical of ZnO-coated $LiNi_{0.8}Co_{0.15}Al_{0.05}O_2$ cathodes. The synergistic action of Ni^{2+} preoxidation by $(NH_4)_2S_2O_8$ and the optimization of calcination temperature reduced the cation mixing of $LiNi_{0.8}Co_{0.15}Al_{0.05}O_2$. The solid-phase Al-doping improved the uniformity of element distribution and the orderliness of the layered structure. In addition, the surface of $LiNi_{0.8}Co_{0.15}Al_{0.05}O_2$ was coated with ZnO [27,28] which improved the structural stability and cycling performance. The preparation process of ZnO-coated $LiNi_{0.8}Co_{0.15}Al_{0.05}O_2$ is shown in Figure 1.

2 Experimental

2.1 Preparation of $LiNi_{0.8}Co_{0.15}Al_{0.05}O_2$

The $NiSO_4{\cdot}6H_2O$ and $CoSO_4{\cdot}7H_2O$ (molar ratio of 0.80:0.15) were dissolved in deionized water to form a mixed salt solution at a concentration of 1.9 mol L^{-1} and added a certain amount of $(NH_4)_2S_2O_8$ solution. 4 mol L^{-1} NaOH solution and 1.5 mol L^{-1} $NH_3{\cdot}H_2O$ solution are served as the pH control agent and the chelating agent, respectively. The $NH_3{\cdot}H_2O$ solution is first added to a 5 L reactor, and then the salt solution and the NaOH solution are pumped together into the reactor at a flow rate ratio of 2:1 to react at 50°C for 30 h; the pH was controlled at 11.00 ± 0.02 by an online pH meter. Then, the $Ni_{0.8}Co_{0.15}(OH)_2$ was obtained after washing and drying. Subsequently, solid-phase Al-doping is used to prepare the $LiNi_{0.8}Co_{0.15}Al_{0.05}O_2$. The Li_2CO_3, $Ni_{0.8}Co_{0.15}(OH)_{1.9}$, and $Al(NO_3)_3{\cdot}9H_2O$ (molar ratio of Li:Ni:Co:Al = 1.08:0.8:0.15:0.05) were mixed and ball-milled for 5 h, then calcined at 500°C for 5 h under the oxygen atmosphere in a tube furnace to obtain the intermediate product. After that, the intermediate product is cooled to room temperature, ball-milled for 5 h, placed in the tube furnace again, and calcined at 750°C for 12 h in the oxygen atmosphere to form $LiNi_{0.8}Co_{0.15}Al_{0.05}O_2$.

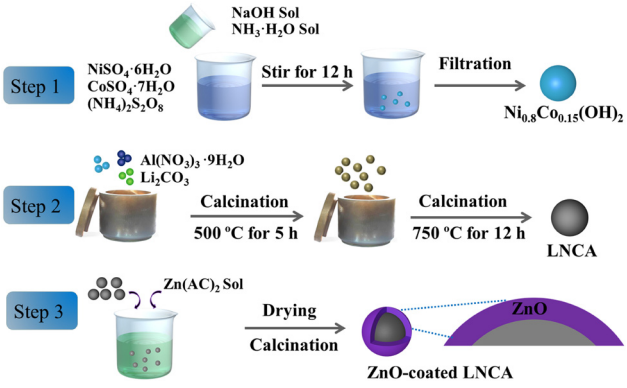

Figure 1: Schematic view of the synthesis process of ZnO-coated $LiNi_{0.8}Co_{0.15}Al_{0.05}O_2$.

2.2 Preparation of ZnO-coated $LiNi_{0.8}Co_{0.15}Al_{0.05}O_2$

A certain amount of $Zn(AC)_2{\cdot}2H_2O$ was dissolved in 40 mL of ethanol, and after ultrasonic dissolution, 2 g of the $LiNi_{0.8}Co_{0.15}Al_{0.05}O_2$ obtained in the above step was added under vigorous stirring for 4 h, and then increased to 65°C to evaporate the ethanol. The mixture was dried at 120°C for 12 h, and finally calcined at 450°C for 5 h to obtain ZnO-coated $LiNi_{0.8}Co_{0.15}Al_{0.05}O_2$ powder which could be used as cathode material. The amount of $Zn(AC)_2{\cdot}2H_2O$ added to prepare ZnO-coated $LiNi_{0.8}Co_{0.15}Al_{0.05}O_2$ were 1, 2, 3 wt%, and the prepared samples were recorded as Z1, Z2, and Z3, respectively, and the pristine $LiNi_{0.8}Co_{0.15}Al_{0.05}O_2$ as Z0.

2.3 Materials characterization

The material structure was analyzed by X-ray powder diffractometer (XRD, Ultima type, Japan Science) at the scanning speed of $0.2°\ s^{-1}$ with the scanning range of 10–80°. Thermogravimetric (TG) measurements (Netzsch-STA 449C) were conducted from room temperature to 900°C at a heating rate of $10°C\ min^{-1}$ in air. The surface morphology was analyzed by scanning electron microscope (SEM, Zeiss supra 55, Zeiss, Germany) and transmission electron microscopy (TEM, JEM-2100HR, Japan).

2.4 Electrochemical measurements

The working electrodes were prepared by mixing active material, acetylene black, and PVDF at a mass ratio of 8:1:1 in *N*-methylpyrrolidinone solution. The slurry was coated onto the aluminum foil and dried at 110°C for 5 h. Then the coated foil was pressed and punched into 14 mm diameter disks. The electrodes were transferred to a glove box (Super 1220/750, Mikrouna Co., Ltd. China) to assemble in 2025 coin-type cells with a lithium foil counter electrode. Celgard-2400 was used as the separator and 1 M $LiPF_6$ dissolved in ethylene carbonate (EC) and diethyl carbonate (DEC) (1:1 in volume ratio) as the electrolyte solution.

The galvanostatic charge and discharge cycle were conducted on CT2001A (LAND, Bart Rui Tech. Co., Ltd.) battery test system between 2.8 and 4.3 V (*vs* Li/Li^+) under different current densities. Cyclic voltammetry (CV) test was recorded on Gamry electrochemical system (Interface1010E) with a potential range of 3.0–4.3 V (*vs* Li/Li^+) at a scanning rate of $0.1\ mV\ s^{-1}$. Electrochemical impedance spectrum (EIS, 100 kHz to 0.01 Hz) was performed using the same electrochemical system.

3 Results and discussion

3.1 Effect of different calcination temperatures on $LiNi_{0.8}Co_{0.15}Al_{0.05}O_2$

As known, the crystal structures and microstructures of $LiNi_{0.8}Co_{0.15}Al_{0.05}O_2$ are also affected by the calcination temperature. Therefore, to determine the calcination temperature for preparing $LiNi_{0.8}Co_{0.15}Al_{0.05}O_2$, the thermogravimetric analysis (TGA) was conducted in air for the mixture Li_2CO_3, $Ni_{0.8}Co_{0.15}(OH)_{1.9}$, and $Al(NO_3)_3{\cdot}9H_2O$ (molar ratio of Li:Ni:Co:Al = 1.08:0.8:0.15:0.05) in the temperature range from 25 to 900°C, as shown in Figure 2. The differential curve is the relationship between the temperature and the first derivative of time in the TG curve, which represents the weight loss rate. It can be seen that there is a slow weight loss from room temperature to 90°C, corresponding to a small endothermic peak (a) on the differential curve, which is due to weight loss of absorbed water on surface and crystal water of $Al(NO_3)_3$. A dramatic decline occurs from 190 to 270°C, corresponding to the maximum endothermic peak of the differential curve (b), mainly ascribed to the process of $Ni_{0.8}Co_{0.15}(OH)_{1.9}$ forming $Ni_{0.8}Co_{0.15}O_2$. From 270 to 500°C, there is a relatively slow weight loss, corresponding to the broad endothermic peak (c) on the differential curve, which is due to the thermal decomposition of Li_2CO_3 to produce Li_2O and release CO_2. With the further increase in temperature,

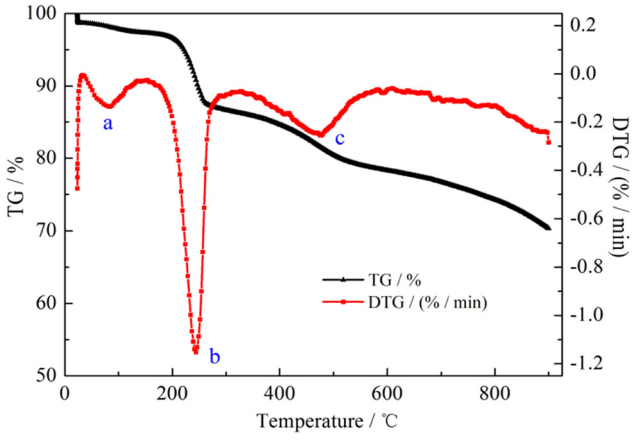

Figure 2: TG–DTG curve of the mixture of Li_2CO_3, $Ni_{0.8}Co_{0.15}(OH)_{1.9}$, and $Al(NO_3)_3{\cdot}9H_2O$.

Al_2O_3 was formed by decomposition of $Al(NO_3)_3$, and finally $LiNi_{0.8}Co_{0.15}Al_{0.05}O_2$ was synthesized. The analytical curve shows that the thermal reaction of the mixture is carried out in stages. In order to obtain a positive cathode material with excellent performance, it is necessary to strictly control the calcination conditions. In addition, when the temperature is around 850°C, there is a slow weight loss, due to the volatilization of lithium, thereby, the calcination temperature cannot exceed 850°C.

Figure 3 shows the XRD patterns of the samples prepared at different calcination temperatures. All peaks are well-indexed to the *R*3*m* group and consistent with the layered structure of α-$NaFeO_2$ [29]. Two pairs of splitting peaks, (006/102) and (108/110), in the XRD patterns correspond to the typical structural features of hexagonal layered materials [30]. None of the four samples show any impurity peaks, proving that the pure phase of $LiNi_{0.8}Co_{0.15}Al_{0.05}O_2$ for cathode material was synthesized. As the temperature rises, the intensity of the (108/110) peak and (006/102) peak increases, indicating that the increase in the calcination temperature improves the crystallinity of the samples. The lattice parameters of the four samples are shown in Table 1. It can be seen that the calcination temperature has little effect on the lattice parameters of *a*, *c*, and *V*, but has a certain influence on the ratio of I_{003}/I_{104}. In the ternary cathode material, the ratio of I_{003}/I_{104} corresponds to the internal cation mixing, and the sample calcined at 750°C has the largest ratio of I_{003}/I_{104}, and the corresponding cation mixing is the smallest. Therefore, the calcination temperature of 750°C is the most suitable.

Figure 4 shows the cycling performance of $LiNi_{0.8}Co_{0.15}Al_{0.05}O_2$ prepared at different calcination temperatures in the voltage range of 2.8–4.3 V at 0.2C. It can be seen that the discharge capacity generally improves with the increasing calcination temperature at first, and then tends to decline. The sample synthesized at 750°C has a higher initial discharge-specific capacity of 186.8 mA h g^{-1} with a capacity retention of 83.6% after 50 cycles, which is better than that of the samples prepared at 700°C (183.8 mA h g^{-1}, 80.5%) and 800°C (185.8 mA h g^{-1}, 78.5%). When the temperature reached 850°C, a quick capacity fading is observed (from 175.3 to 137.1 mA h g^{-1}). In summary, the experimental results prove that the sample obtained at the calcination temperature of 750°C has the best cycling performance and higher discharge-specific capacity, which is consistent with the XRD results.

Table 1: Lattice parameters of $LiNi_{0.8}Co_{0.15}Al_{0.05}O_2$ prepared at different calcination temperatures

Sample/°C	*a*/Å	*c*/Å	*c*/*a*	*V* (Å × 10^3)	I_{003}/I_{104}
700	2.86112	14.16892	4.9433	101.31	1.51
750	2.86232	14.16877	4.9421	101.23	1.79
800	2.86332	14.16965	4.9488	101.87	1.52
850	2.86375	14.16433	4.9367	101.53	1.74

3.2 Effect of ZnO coating on $LiNi_{0.8}Co_{0.15}Al_{0.05}O_2$

Since ZnO has relatively high electron mobility and low cost, the as-prepared $LiNi_{0.8}Co_{0.15}Al_{0.05}O_2$ was coated with ZnO to improve the structural stability and cycling performance. Figure 5a is the XRD patterns of the Z0, Z1, Z2, and Z3, showing that the XRD patterns of the four

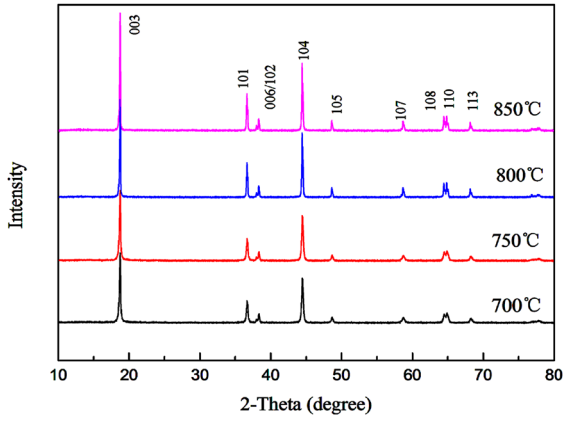

Figure 3: XRD pattern of $LiNi_{0.8}Co_{0.15}Al_{0.05}O_2$ prepared at different calcination temperatures.

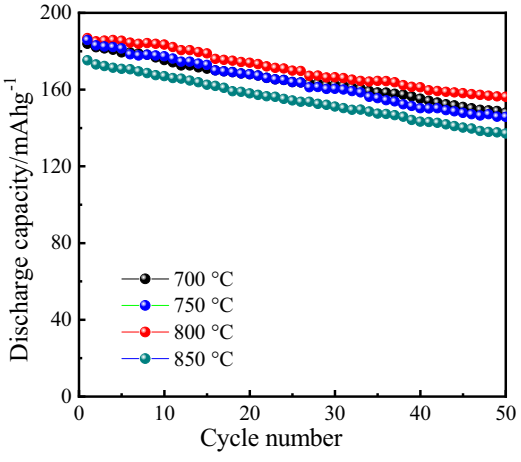

Figure 4: Cycling performance of $LiNi_{0.8}Co_{0.15}Al_{0.05}O_2$ prepared at different calcination temperatures.

samples are basically the same. Compared with the standard XRD pattern of ZnO (Figure 5b), there is no characteristic peak of ZnO appeared in the XRD pattern of Z1, Z2, and Z3 because the amount of ZnO used in modification is very small and beyond the XRD resolution. The lattice parameters of the four samples are listed in Table 2. There is no significant change in the lattice constants for pristine (Z0) and coated samples (Z1, Z2 and Z3), indicating that the Zn^{2+} does not enter the host structure of $LiNi_{0.8}Co_{0.15}Al_{0.05}O_2$. The ratio of I_{003}/I_{104} for the coated samples is larger than that of pristine sample, indicating that ZnO-coated layer reduces the cation mixing of $LiNi_{0.8}Co_{0.15}Al_{0.05}O_2$ [31].

Figure 6 shows the cycling performance of Z0, Z1, Z2, and Z3 at 0.2C in the voltage range of 2.8–4.3 V. It can be seen that the discharge capacity of pristine sample fades from 186.8 to 146.5 mA h g^{-1} after 100 cycles with a capacity retention of 78.4%. In contrast, the ZnO-coated samples remain 91.3, 90.2, and 86.6% for Z1, Zn2, and Z3 after 100 cycles, respectively, which demonstrates that the ZnO-coated samples have higher cyclic stability than pristine samples. The reason for the improvement of cycling performance is that ZnO-coated layer works as an isolating layer, which effectively reduces the side reactions between electrode and electrolyte, inhibits the internal collapse of the structure caused by the dissolution of transition metals [32], improves the structural stability of the material, and further improves the cycling performance of $LiNi_{0.8}Co_{0.15}Al_{0.05}O_2$ cathode material. In addition, the thin ZnO-coated layer can improve the diffusion rate of Li^+ and the conductivity of the electrode. This result will be verified by CV and EIS. However, the cycling performance of Z2 and Z3 is slightly lower than that of Z1 after 100 cycles, indicating that the thick coating will hinder the diffusion of Li^+ to a certain extent.

Table 2: Lattice parameters of pristine and ZnO-coated $LiNi_{0.8}Co_{0.15}Al_{0.05}O_2$ samples

Sample	a/Å	c/Å	c/a	V (Å^3)	I_{003}/I_{104}
Z0	2.866232	14.16877	4.9433	101.31	1.79
Z1	2.866239	14.16253	4.9430	101.37	1.81
Z2	2.86210	14.17036	4.9435	101.46	1.89
Z3	2.86256	14.17508	4.9440	101.57	1.83

Figure 7 is the SEM image of pristine and 1 wt% ZnO-coated $LiNi_{0.8}Co_{0.15}Al_{0.05}O_2$. The pristine sample is spherical particles with a clean surface (Figure 7a), and the secondary particles are formed by primary particle aggregation (Figure 7b). In contrast, the surface of the ZnO-coated $LiNi_{0.8}Co_{0.15}Al_{0.05}O_2$ spheres became obviously rough, and there were many needle-liked nano-rods and channels on the surface (Figure 4c and d), which expand the tunnels for Li^+ diffusion and also stabilize the $LiNi_{0.8}Co_{0.15}Al_{0.05}O_2$ frame, proving that the ZnO successfully attached to the $LiNi_{0.8}Co_{0.15}Al_{0.05}O_2$ surface.

More detailed structural features of the pristine and 1 wt% ZnO-coated $LiNi_{0.8}Co_{0.15}Al_{0.05}O_2$ were explored by high-resolution TEM. The pristine sample shows smooth surface and clear lattice fringes, indicating high crystallization (Figure 8a). The inter planar distance of pristine sample is about 0.47 nm (Figure 8b), corresponding to the planar distance of the (003) plane in XRD patterns [33]. As shown in Figure 8c and d, it is obvious that the ZnO nanoparticles are attached to the surface of the $LiNi_{0.8}Co_{0.15}Al_{0.05}O_2$, which is consistent with the result of the SEM image. As anticipated, this coating layer should improve electrochemical performances of $LiNi_{0.8}Co_{0.15}Al_{0.05}O_2$ by protecting its surface from electrolyte corrosion and HF attack.

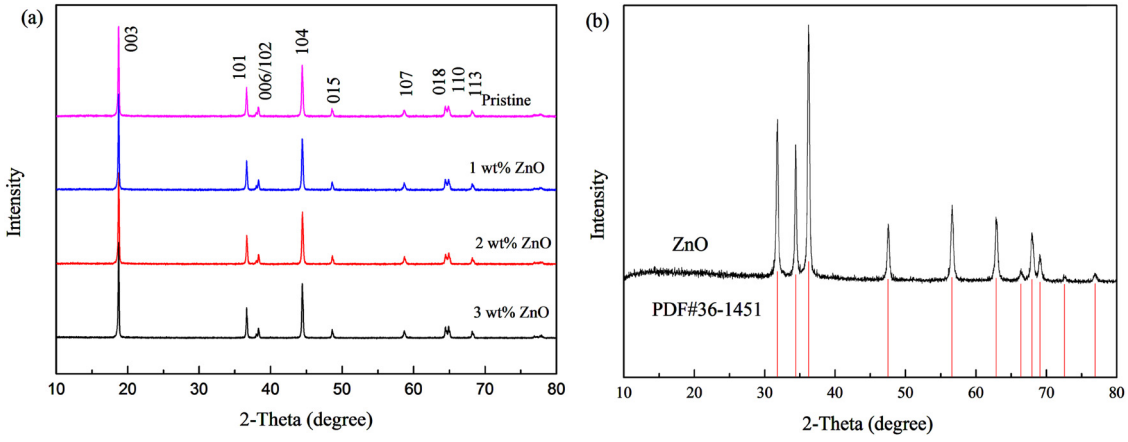

Figure 5: (a) XRD patterns of the pristine and ZnO-coated $LiNi_{0.8}Co_{0.15}Al_{0.05}O_2$, (b) standard XRD pattern of ZnO.

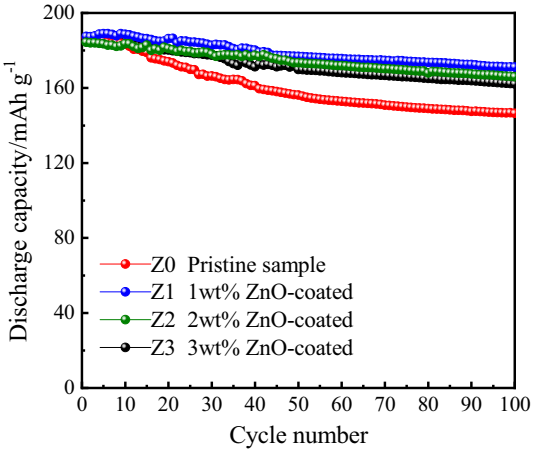

Figure 6: Cycling performance of the pristine and ZnO-coated $LiNi_{0.8}Co_{0.15}Al_{0.05}O_2$ samples at 0.2C.

The rate performance tests of pristine and ZnO-coated $LiNi_{0.8}Co_{0.15}Al_{0.05}O_2$ were conducted under different current rates (0.2, 0.5, 1, 3, 5, 10C) in the voltage range of 2.8–4.3 V. As shown in Figure 9, at a low current rate of 0.2C, the discharge capacity of the ZnO-coated $LiNi_{0.8}Co_{0.15}Al_{0.05}O_2$ is not significantly improved. However, as the current density increases, the rate performance of ZnO-coated $LiNi_{0.8}Co_{0.15}Al_{0.05}O_2$ is obviously better than that of the pristine one. At the current rate of 10C, ZnO-coated $LiNi_{0.8}Co_{0.15}Al_{0.05}O_2$ shows a higher discharge capacity of 135 mA h g^{-1} than that of the pristine sample (115 mA h g^{-1}). In general, the ZnO-coated $LiNi_{0.8}Co_{0.15}Al_{0.05}O_2$ has ZnO protective layer, which can reduce the interfacial impedance, inhibit the electrochemical polarization, and hence improve the rate performance.

Figure 10 shows the CV of the pristine and ZnO-coated $LiNi_{0.8}Co_{0.15}Al_{0.05}O_2$ after 10 cycles with a scanning rate of 0.1 mV s^{-1} in a voltage range of 3.0–4.3 V. Those two curves show the unique redox couples of Nickel-based compounds [34]. The three pairs of redox peaks from left to right correspond to Ni^{2+}/Ni^{3+}, Ni^{3+}/Ni^{4+}, and Co^{3+}/Co^{4+} [35]. In the anodic process, the peak located at about 3.76 V corresponds to phase transition from the hexagonal phase (H1) to the monoclinic phase (M), the peak at about 4.00 V corresponds to the phase transition from M to a new hexagonal phase (H2), and the peak at about 4.18 V corresponds to the phase transition from the H2 to another hexagonal phase (H3) [36]. There is no other peak in the curves of the ZnO-coated $LiNi_{0.8}Co_{0.15}Al_{0.05}O_2$, indicating that the modification of ZnO does not affect the structure of $LiNi_{0.8}Co_{0.15}Al_{0.05}O_2$ cathode material.

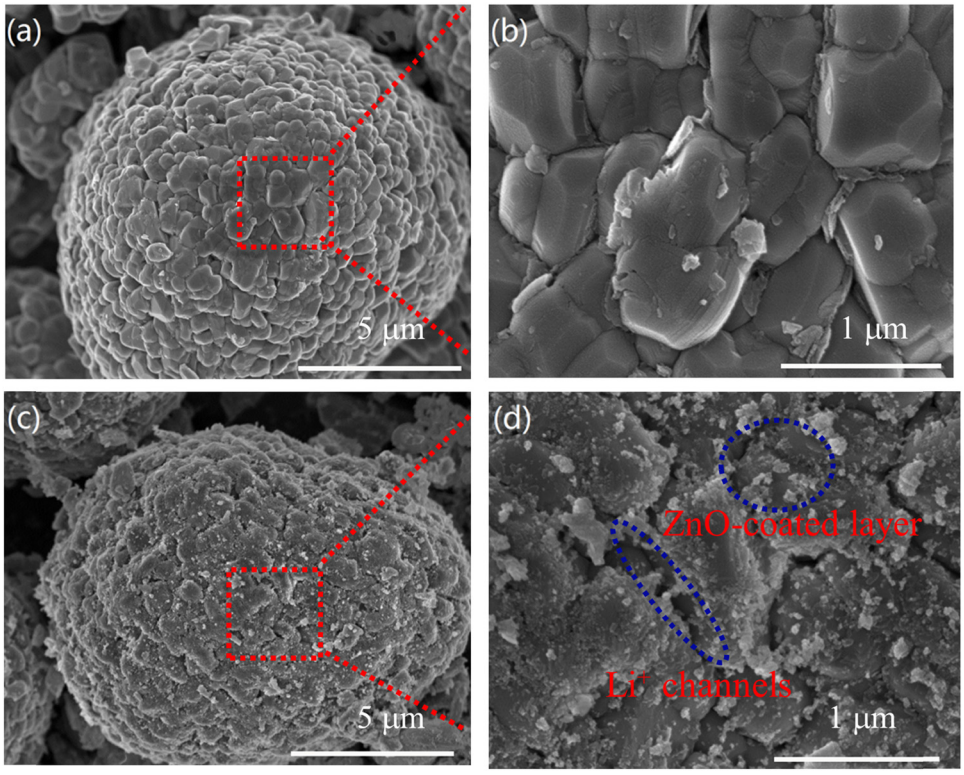

Figure 7: SEM images of the (a and b) pristine and (c and d) 1 wt% ZnO-coated $LiNi_{0.8}Co_{0.15}Al_{0.05}O_2$ samples.

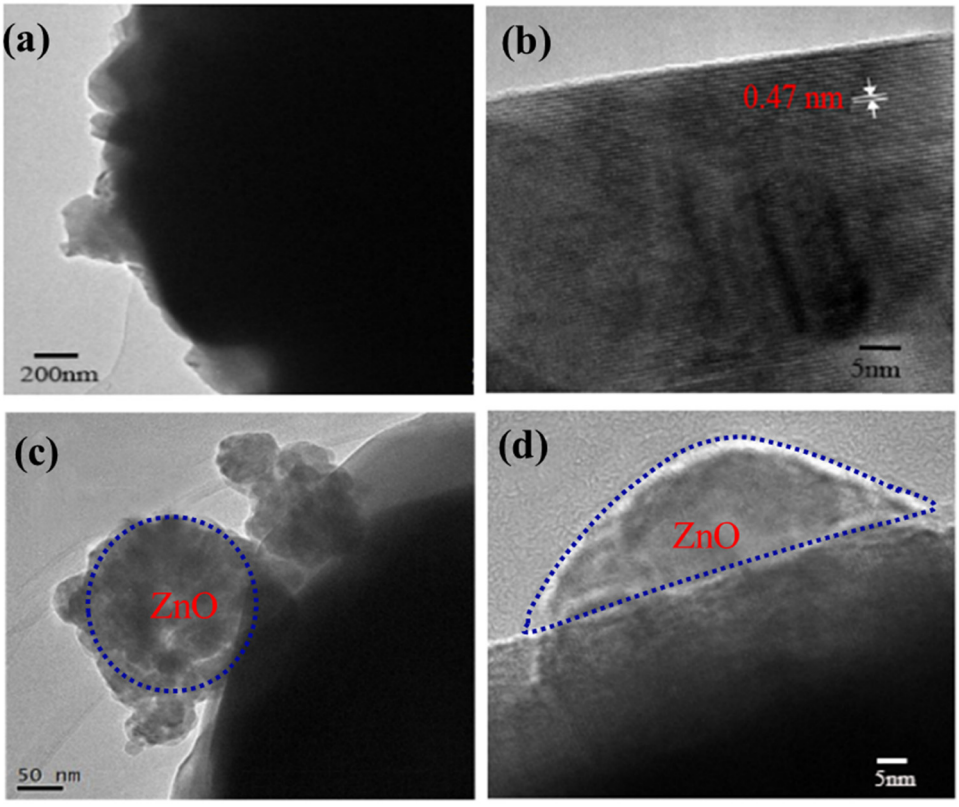

Figure 8: TEM images of (a and b) pristine and (c and d) ZnO-coated $LiNi_{0.8}Co_{0.15}Al_{0.05}O_2$.

To further investigate the reasons for the improvement of rate performance, the CV measurements were performed at various scanning rates. The potential intervals (ΔV) between the anodic and cathodic peaks indicate the reversibility of Li^+ insertion/extraction and electrode polarization [37]. As shown in Figure 11a and b, ΔV increases with the increase of the scanning rate, and when the scanning rate is 0.8 mV s^{-1}, the ΔV of the main peak (Ni^{3+}/Ni^{4+}, located at about 3.8 V) of ZnO-coated $LiNi_{0.8}Co_{0.15}Al_{0.05}O_2$ is 0.37 V, smaller than that of the pristine sample (0.43 V), which indicated that the modification of ZnO can inhibit the electrode polarization and improve the electrochemical reversibility [38]. As shown in Figure 11c and d, the linear relationship between the redox peak current (i_p) and the square root of

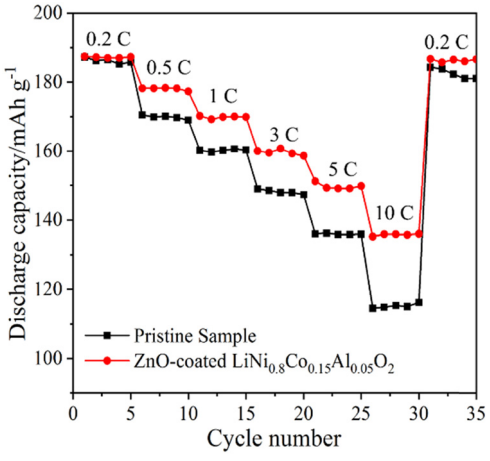

Figure 9: Rate performance of pristine and ZnO-coated $LiNi_{0.8}Co_{0.15}Al_{0.05}O_2$ samples.

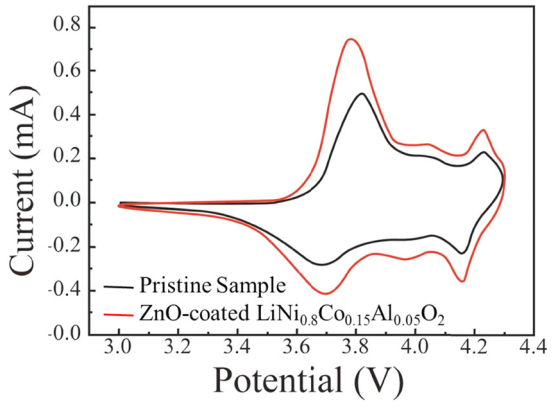

Figure 10: CV curves of pristine and ZnO-coated $LiNi_{0.8}Co_{0.15}Al_{0.05}O_2$ samples at a scanning rate of 0.1 mV s^{-1} in the voltage of 3.0–4.3 V.

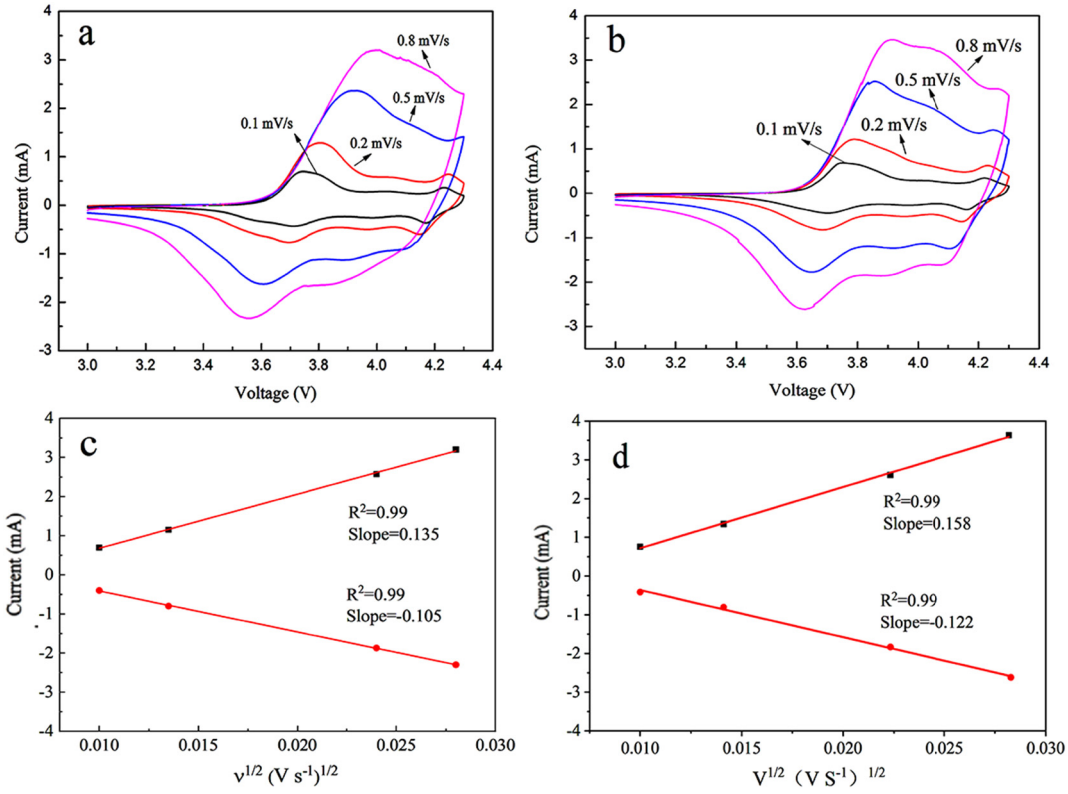

Figure 11: Cyclic voltammogram of (a) pristine and (b) ZnO-coated $LiNi_{0.8}Co_{0.15}Al_{0.05}O_2$ at various scanning rates; linear relationship between the peak currents (i_p) and square root of scan rate ($v^{1/2}$): (c) pristine sample, (d) ZnO-coated $LiNi_{0.8}Co_{0.15}Al_{0.05}O_2$ sample.

scanning rate ($v^{1/2}$) is employed to calculate the Li^+ diffusion coefficient (D_{Li^+}) of the main peak (Ni^{3+}/Ni^{4+}, located at about 3.7 V), which is the same method used in the literature [39]. The D_{Li^+} is calculated by the following equation:

$$i_p = 2.69 \times 10^5 n^{3/2} A D_{Li}^{1/2} C^* v^{1/2}$$

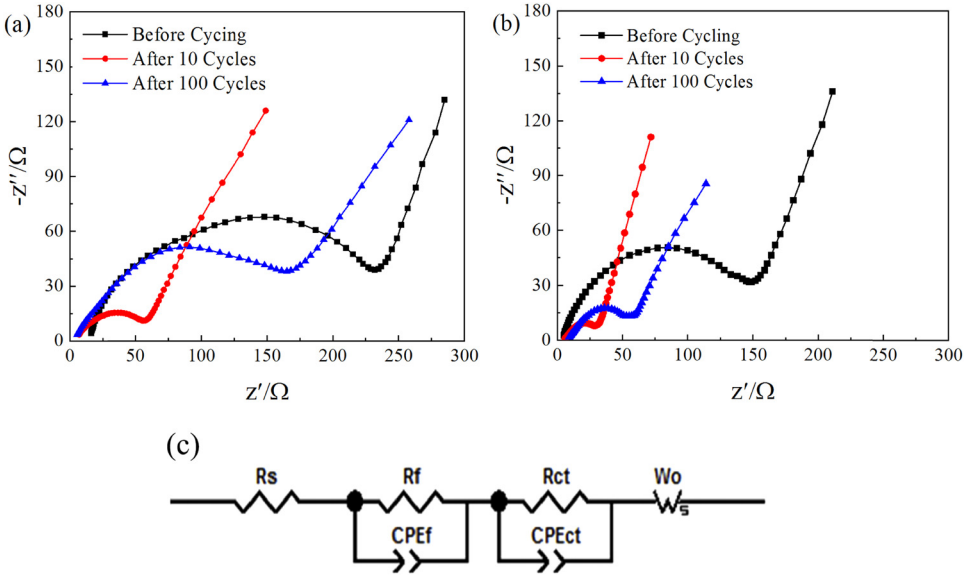

Figure 12: Nyquist plots of (a) pristine and (b) ZnO-coated $LiNi_{0.8}Co_{0.15}Al_{0.05}O_2$ samples after different cycles, (c) equivalent circuit model.

Table 3: EIS parameters of pristine and ZnO-coated $LiNi_{0.8}Co_{0.15}Al_{0.05}O_2$ after different cycles

Sample	Cycle number	R_s (Ω)	R_f (Ω)	R_{ct} (Ω)
$LiNi_{0.8}Co_{0.15}Al_{0.05}O_2$	0	5.825	15.456	233.31
	10	3.164	12.146	65
	100	4.163	16.428	172.5
ZnO-coated	0	4.125	14.943	151
$LiNi_{0.8}Co_{0.15}Al_{0.05}O_2$	10	2.823	6.962	28
	100	3.426	10.944	62.8

where, the n is charge-transfer number, and C^* is the concentration of Li^+ in the active material. The D_{Li^+} at the oxidation peak and the reduction peak of the initial sample are 1.89×10^{-10} and 1.47×10^{-10} $cm^2 s^{-1}$, respectively, which is smaller than that of ZnO-coated $LiNi_{0.8}Co_{0.15}Al_{0.05}O_2$ (2.21×10^{-10} and 1.71×10^{-10} $cm^2 s^{-1}$). The diffusion control dominates the electrochemical reaction during the Li^+ insertion/extraction progress. Therefore, the modification of ZnO improves the rate performance.

Figure 12 shows the Nyquist plots of the pristine and ZnO-coated $LiNi_{0.8}Co_{0.15}Al_{0.05}O_2$ samples before and after 10 and 100 cycles. The equivalent circuit model of the studied system is also shown in Figure 9d. R_s represents the resistance of the electrolyte, R_f means the surface film resistance, R_{ct} is the charge-transfer resistance [40], and W is the Warburg impedance that reflects the diffusion of Li^+ in the solid [41].

All the fitted EIS parameters are listed in Table 3. It is noted that these two samples both show a large R_{ct} value before cycling, which is caused by the inactivation of the electrodes [42]. As the cycling test begins, the R_{ct} value decreases rapidly during the internal activation process [43]. However, after 100 cycles, the R_{ct} value of the pristine sample quickly increased to 172.5 Ω, which was much higher than that of after 10th cycle. However, the value of R_{ct} for ZnO-coated $LiNi_{0.8}Co_{0.15}Al_{0.05}O_2$ after 100 cycles is only about 62.8 Ω, much smaller than that of the pristine one. It can be concluded from the experimental results that the ZnO-coated layer decreases the charge-transfer resistance, increases the electronic conductivity of $LiNi_{0.8}Co_{0.15}Al_{0.05}O_2$, and further improves the rate performance.

4 Conclusion

In conclusion, we designed a novel method for the preparation of high-capacity $LiNiO_2$-based cathode materials. First of all, the addition of $(NH_4)_2S_2O_8$ reduces the cation mixing of $LiNi_{0.8}Co_{0.15}Al_{0.05}O_2$; solid-phase Al-doping improves the element distribution and layered structure. Then, optimizing the calcination temperature enhances the crystallinity of $LiNi_{0.8}Co_{0.15}Al_{0.05}O_2$, and the ZnO was coated on the surface of $LiNi_{0.8}Co_{0.15}Al_{0.05}O_2$ to improve the cycling performance. The electrochemical tests demonstrated a high reversible discharge capacity of 172.1 mA h g^{-1} at 0.2C with the capacity retention of 91.3% after 100 cycles and a good rate performance at high current density. The above-mentioned improvement indicates the potential application of ZnO-coated $LiNi_{0.8}Co_{0.15}Al_{0.05}O_2$ as the cathode material for advanced LIBs.

Funding information: This research was financially supported by Minjiang Scholarship of Fujian Province (No. Min-Gaojiao[2010]-117), Central-government Guided Fund for Local Economic Development (No. 830170778), R&D Fund for Strategic Emerging Industry of Fujian Province (No. 82918001), and International Cooperation Project of Fujian Science and Technology Department (No. 830170771).

Author contributions: All authors have accepted responsibility for the entire content of this manuscript and approved its submission.

Conflict of interest: David Hui, who is the coauthor of this article, is a current Editorial Board member of *Nanotechnology Reviews*. This fact did not affect the peer-review process. The authors declare no other conflict of interest.

References

[1] Lin D, Liu Y, Cui Y. Reviving the lithium metal anode for high-energy batteries. Nat Nanotechnol. 2017;12:194–206.
[2] Cano ZP, Banham D, Ye S, Hintennach A, Lu J, Fowler M, et al. Batteries and fuel cells for emerging electric vehicle markets. Nat Energy. 2018;3:279–89.
[3] Pfleging W. A review of laser electrode processing for development and manufacturing of lithium-ion batteries. Nanotechnol Rev. 2018;7(3):549–73.
[4] Lee MJ, Noh M, Park MH, Jo M, Kim H, Nam H, et al. The role of nanoscale-range vanadium treatment in $LiNi_{0.8}Co_{0.15}Al_{0.05}O_2$ cathode materials for Li-ion batteries at elevated temperatures. J Mater Chem. 2015;3:13450–53.
[5] Gao S, Cheng YT, Shirpour M. Effects of cobalt deficiency on nickel-rich layered $LiNi_{0.8}Co_{0.1}Mn_{0.1}O_2$ positive electrode materials for lithium-ion batteries. ACS Appl Mater Inter. 2019;11:982–9.

[6] Novikova SA, Yaroslavtsev AB. Cathode materials based on olivine lithium iron phosphates for lithium-ion batteries. Rev Adv Mater Sci. 2017;49(2):129–39.
[7] Augustyn V, Therese S, Turner TC, Manthiram A. Nickel-rich layered $LiNi_{1-x}M_xO_2$ (M = Mn, Fe, and Co) electrocatalysts with high oxygen evolution reaction activity. J Mater Chem. 2015;3:16604–12.
[8] Shi JL, Xiao DD, Zhang XD, Yin YX, Guo YG, Gu L, et al. Improving the structural stability of Li-rich cathode materials via reservation of cations in the Li-slab for Li-ion batteries. Nano Res. 2017;12:1–9.
[9] Li LJ, Chen ZY, Zhang QB, Xu M, Zhou X, Zhu HL, et al. A hydrolysis-hydrothermal route for the synthesis of ultrathin $LiAlO_2$-inlaid $LiNi_{0.5}Co_{0.2}Mn_{0.3}O_2$ as a high-performance cathode material for lithium ion batteries. J Mater Chem. 2015;3:894–904.
[10] Makimura Y, Sasaki T, Nonaka T, Nishimura YF, Uyama T, Okuda C, et al. Factors affecting cycling life of $LiNi_{0.8}Co_{0.15}Al_{0.05}O_2$ for lithium-ion batteries. J Mater Chem. 2016;4:8350–58.
[11] Zhang HZ, Liu C, Song DW, Zhang LQ, Bie LJ. A new synthesis strategy towards enhancing the structure and cycle stabilities of the $LiNi_{0.80}Co_{0.15}Al_{0.05}O_2$ cathode material. J Mater Chem. 2017;5:835–41.
[12] Wu NT, Wu H, Yuan W, Liu SJ, Liao JY, Zhang Y, et al. Facile synthesis of one-dimensional $LiNi_{0.9}Co_{0.07}Al_{0.03}O_2$ microrods as advanced cathode materials for lithium ion batteries. J Mater Chem. 2015;3:13648–52.
[13] Song X, Liu GX, Yue HF, Luo L, Yang SY, Huang YY, et al. A novel low-cobalt long-life $LiNi_{0.88}Co_{0.06}Mn_{0.03}Al_{0.03}O_2$ cathode material for lithium ion batteries. Chem Eng J. 2020;407:126301–10.
[14] Liu W, Oh P, Liu X, Lee MJ, Cho W, Chae S, et al. Nickel-rich layered lithium transition-metal oxide for high-energy lithium-ion batteries. Angew Chem Int Ed. 2015;127:4518–36.
[15] Chen M, Zhao EY, Chen DF, Wu MM, Han SB, Huang QZ, et al. Decreasing Li/Ni disorder and improving the electrochemical performances of Ni-Rich $LiNi_{0.8}Co_{0.1}Mn_{0.1}O_2$ by Ca doping. Inorg Chem. 2017;56:8355–62.
[16] Jo M, Noh M, Oh P, Kim Y, Cho J. A new high power $LiNi_{0.81}Co_{0.1}Al_{0.09}O_2$ cathode material for lithium-ion batteries. Adv Energy Mater. 2014;4:1301583.
[17] Chen WH, Li YY, Yang D, Feng XM, Guan XX, Mi LW, et al. Controlled synthesis of spherical hierarchical $Li–Ni_{1-x-y}Co_xAl_yO_2$ ($0 < x, y < 0.2$) via a novel cation exchange process as cathode materials for high-performance lithium batteries. Electrochim Acta. 2016;190:932–38.
[18] Bak SM, Nam KW, Chang WY, Yu XQ, Hu EY, Hwang S, et al. Correlating structural changes and gas evolution during the thermal decomposition of charged $Li_xNi_{0.8}Co_{0.15}Al_{0.05}O_2$ cathode materials. Chem Mater. 2013;25:337–51.
[19] Trease NM, Seymour ID, Radin MD, Liu H, Hao L, Hy S, et al. Identifying the distribution of Al^{3+} in $LiNi_{0.8}Co_{0.15}Al_{0.05}O_2$. Chem Mater. 2016;28(22):870–80.
[20] Liang M, Song D, Zhang H. Improved performances of $LiNi_{0.8}Co_{0.15}Al_{0.05}O_2$ material employing $NaAlO_2$ as a new aluminium source. ACS Appl Mater Inter. 2017;9:7b12306.
[21] Zhou P, Meng H, Zhang Z, Chen CC, Lu Y, Cao J, et al. Stable layered Ni-rich $LiNi_{0.9}Co_{0.07}Al_{0.03}O_2$ microspheres assembled with nanoparticles as high-performance cathode materials for lithium-ion batteries. J Mater Chem A Mater Energ Sus. 2017;5(6):2724–31.
[22] Kim Y, Kim D. Synthesis of high-density nickel cobalt aluminum hydroxide by continuous coprecipitation method. ACS Appl Mater Inter. 2012;4(2):586.
[23] Zhang W, Chi ZX, Mao WX, Lv RW, Cao AM, Wan LJ, et al. One-nanometer-precision control of Al_2O_3 nanoshell through solution-based synthesis route. Angew Chem Int Ed. 2014;53:12776–80.
[24] Zhu B, Liu N, Mcdowell M, Jin Y, Cui Y, Zhu J, et al. Interfacial stabilizing effect of ZnO on Si anodes for lithium ion battery. Nano Energy. 2015;13:620–25.
[25] Liang L, Hu G, Jiang F, Cao Y. Electrochemical behaviours of SiO_2-coated $LiNi_{0.8}Co_{0.1}Mn_{0.1}O_2$ cathode materials by a novel modification method. J Alloy Compound. 2016;657:570–81.
[26] Liu X, Wang S, Wang L, Wang K, Wu XZ, Zhou PF, et al. Stabilizing the high-voltage cycle performance of $LiNi_{0.8}Co_{0.1}Mn_{0.1}O_2$ cathode material by Mg doping. J Power Sources. 2019;438(31):227017–24.
[27] Yu W, Huang L, Yang D, Fu P, Zhou L, Zhang J, et al. Efficiency exceeding 10% for inverted polymer solar cells with a ZnO/ionic liquid combined cathode interfacial layer. J Mater Chem. 2015;A310:660–65.
[28] Huang XR, Zeng LJ, Li RF, Xi ZJ, Li YC. Manipulating conductive network formation via 3D T-ZnO: A facile approach for a CNT-reinforced nanocomposite. Nanotechnol Rev. 2020;9:534–42.
[29] Fu CC, Li GS, Luo D, Li Q, Fan JM, Li LP, et al. Nickel-rich layered microspheres cathodes: lithium/nickel disordering and electrochemical performance. ACS Appl Mater Inter. 2014;6:15822–31.
[30] Yu HJ, Qian YM, Otani M, Tang DM, Guo SH, Zhu YB, et al. Study of the lithium/nickel ions exchange in the layered $LiNi_{0.42}Mn_{0.42}Co_{0.16}O_2$ cathode material for lithium ion batteries: experimental and first-principles calculations. Energy Environ Sci. 2014;7:1068–78.
[31] Wu F, Tian J, Su Y, Wang J, Zhang C, Bao L, et al. Effect of Ni(2+) content on lithium/nickel disorder for Ni-rich cathode materials. ACS Appl Mater Inter. 2015;7(14):7702–08.
[32] Zhao EY, Liu XF, Zhao H, Xiao XL, Hu ZB. Ion conducting Li_2SiO_3-coated lithium-rich layered oxide exhibiting high rate capability and low polarization. Chem Commun. 2015;51:9093–96.
[33] Zhao E, Chen M, Chen D, Xiao X, Hu Z. A versatile coating strategy to highly improve the electrochemical properties of layered oxide $LiMO_2$ (M = $Ni_{0.5}Mn_{0.5}$ and $Ni_{1/3}Mn_{1/3}Co_{1/3}$). ACS Appl Mater Inter. 2015;7(49):27096–105.
[34] Qiu Z, Zhang Y, Dong P, Xia S, Yao Y. A facile method for synthesis of $LiNi_{0.8}Co_{0.15}Al_{0.05}O_2$ cathode material. Solid State Ionics. 2017;307:73–8.
[35] Li LJ, Li XH, Wang ZX, Guo HJ, Yue P, Chen W, et al. Synthesis, structural and electrochemical properties of $LiNi_{0.79}Co_{0.1}Mn_{0.1}Cr_{0.01}O_2$ via fast co-precipitation. J Alloys Compd. 2010;507(1):172–77.
[36] Noh HJ, Youn S, Yoon CS, Sun YK. Comparison of the structural and electrochemical properties of layered $Li[Ni_xCo_yMn_z]$-O_2 (x = 1/3, 0.5, 0.6, 0.7, 0.8 and 0.85) cathode material for lithium-ion batteries. J Power Sources. 2013;233:121–30.
[37] Xie H, Hu G, Du K, Peng Z, Cao Y. An improved continuous co-precipitation method to synthesize $LiNi_{0.8}Co_{0.15}Al_{0.05}O_2$ cathode material. J Alloy Compound. 2016;666:84–7.
[38] Rui XH, Ding N, Liu J, Li C, Chen CH. Analysis of the chemical diffusion coefficient of lithium ions in $Li_3V_2(PO_4)_3$ cathode material. Electrochim Acta. 2010;55:2384–90.

[39] Chen CC, Huang YN, An CH, Zhang H, Wang YJ, Jiao LF, et al. Copper-doped dual phase $Li_4Ti_5O_{12}$-TiO_2 nanosheets as high-rate and long cycle life anodes for high-power lithium-ion batteries. ChemSusChem. 2015;8:114–22.
[40] Stenina IA, Kulova TL, Skundin AM, Yaroslavtsev AB. Carbon composites as anode materials for lithium-ion batteries. Rev Adv Mater Sci. 2017;49:140–49.
[41] Reddy MV, Sakunthala A, Pandian SS, Chowdari BVR. Preparation, comparative energy storage properties, and impedance spectroscopy studies of environmentally friendly cathode, $Li(MMn_{11/6})O_4$ (M = $Mn_{1/6}$, $Co_{1/6}$, ($Co_{1/12}Cr_{1/12}$)). J Phys Chem C. 2013;117:9056–64.
[42] Zhang Q, Sha ZF, Cui X, Qiu SQ, He CG, Zhang JL, et al. Incorporation of redox-active polyimide binder into $LiFePO_4$ cathode for high-rate electrochemical energy storage. Nanotechnol Rev. 2020;9:1350–58.
[43] Levi MD, Aurbach D. Impedance of a single intercalation particle and of non-homogeneous, multilayered porous composite electrodes for Li-ion batteries. J Phys Chem B. 2004;108:11693–703.